Energy Conversion and Management 86 (2014) 175–185

Contents lists available at ScienceDirect

Energy Conversion and Management

journal homepage: www.elsevier.com/locate/enconman

A novel all-glass evacuated tubular solar steam generator with simplified CPC

Zhenhua Liu *, Guodong Tao, Lin Lu, Qian Wang

School of Mechanical Engineering, Shanghai Jiao Tong University, Shanghai 200240, China

ARTICLE INFO

Article history:
Received 4 March 2014
Accepted 30 April 2014
Available online 24 May 2014

Keywords:
Solar
Integrated solar system
Steam generator
Heat transfer

ABSTRACT

A low-cost all-glass evacuated tubular solar steam generator with simplified CPC (Compound Parabolic Concentrator) is presented in the paper. It can produce steam exceeding 200 °C with pressure ranging from 0.10 to 0.55 MPa. The solar steam generator primarily consists of 60 collecting units with a total aperture area of 32 m^2 and each unit is comprised of an all-glass evacuated tube, a simplified CPC and a metal concentric annular tube which is inserted into the all-glass evacuated tube. The high viscosity mixture made of high temperature oil and graphite powder is filled in the annular space between the inner glass tube and the copper concentric tube in order to enhance heat transfer from the selective absorbing layer to working fluid flowing in the concentric tube. Outdoor experimental studies have been carried out to investigate the actual performance of the designed solar steam generator in summer time under different operating conditions. Experimental results show that the maximum steam outlet temperature can exceed 200 °C with pressure of 0.55 MPa. The present solar steam generator can steadily produce saturated steam over 150 °C at the pressure range of 0.1–0.55 MPa with a collecting efficiency over 0.30, which can be used as an industrial steam supplier with great potentials for various applications.

1. Introduction

Nowadays the energy demanding is consistently growing, while environmental pollution and destruction caused by fossil fuel is more and more severe. According to the report from International Energy Agency (IEA) in 2011, 81.6% of the world total primary energy supply is from fossil fuel [1]. Renewable energy development and exploration is considered to be an effective way for resolving the contradictory. Solar energy, as one of the easily acquired and viable renewable energy, is currently widely used to generate electricity and produce heat. A study released by International Energy Agency (IEA) on the world energy consumption shows that 45% of the energy demand in 2050 will be provided by solar energy [2].

Among various kinds of utilizations on solar energy, solar steam generation based on solar thermal energy is a quite explicit pattern. Industry consumes nearly one third of the total primary energy, nevertheless almost 60% of the energy is used for heat generation. Industrial Process Heat (IPH) applications usually require the temperature ranges from 60 °C to 260 °C which can be generated by solar energy instead of normal fossil fuels [3,4]. Zahler et al. [5] gave out an application using medium temperature solar steam as heat source instead of typically used gas burner for the curing of paint on the car's body and turned out to achieve good benefits. Medium temperature steam with a relatively high pressure (lower than 1 MPa) can also be applied to textile branch, industrial boilers and mining industry [6,7]. Garcia-Rodriguez et al. [8] proposed an economically multi-effect distillation unit driven by solar steam. Gudekar et al. [9] proposed a pure solar steam generator with CPC for the application of process. Besides, solar steam can be directly used for household which can save lots of expense.

Most solar thermal electricity generation currently is based on parabolic trough solar collectors due to its ability to work at high temperatures up to 400 °C without any serious degradation of efficiency [10]. However, parabolic trough collector (PTC) requires high initial investment, expensive maintenance and operation cost, and usually large-scale area [11]. For power generation by intermediate temperature steam (less than 200 °C and 1.0 MPa), the organic Rankine-like cycle can be deployed; various types of such cycles have been proposed and verified [12]. Ho et al. [13] proposed an organic flash cycle. Their results showed that it can potentially improve the efficiency with intermediate temperature finite thermal sources. Almanza et al. [14] demonstrated that it was possible to generate electricity by medium temperature steam (165 °C, 0.689 MPa) via steam Stuart Swan motor. Ferrara et al. [15] designed a small steam expander reciprocating engine for

* Corresponding author. Tel.: +86 21 34206568.
E-mail address: liuzhenh@sjtu.edu.cn (Z. Liu).

http://dx.doi.org/10.1016/j.enconman.2014.04.099
0196-8904/

Nomenclature

a	half aperture width of a CPC collector, m
A_G	gross area of one collecting unit, m^2
c	coefficient which represents the thermal loss and structural influence of the collector
C_R	concentration ratio of simplified CPC
d	diameter of absorber, m
f_{ref}	multiple reflection coefficients between cover glass tube and inner glass tube
g	gap distance, m
G	solar radiation intensity, W/m^2
h	height of CPC, m
h_f	enthalpy of working fluid, J/kg
Δh_f	enthalpy difference of the collector inlet and outlet, J/kg
l	effective length of CPC, m
$\dot{m}$	mass flow rate of working fluid, kg/s
n	number of collecting units
p	gap loss coefficient
P_{back}	back pressure at the whole system outlet, MPa
P_{in}	pressure at system inlet, MPa
P_{out}	pressure at system outlet, MPa
$\dot{Q}$	instantaneous power output of the system, W
T_i	temperature of the selective coating, °C
T_{outlet}	steam temperature at system outlet, °C
$\dot{V}$	volumetric flow rate of working fluid, L/h
w	width of CPC, m

Greek letters

α_i	absorptivity of selective coating
δ	thickness of copper tube, m
ε_i	emissivity of the selective coating
η_{op}	optical efficiency of CPC
η_{hem}	instantaneous system thermal efficiency
$\overline{\eta_{hem}}$	mean system thermal efficiency
θ_A	acceptance angle of CPC, °
ρ	reflectivity of CPC
ρ_f	denotes density of working fluid, kg/m^3
τ_e	transmissivity of the evacuated tube
τ_d	dust stratification factor of evacuated tube
ϕ	collector slope angle (local latitude), °

Subscripts

CPC	compound parabolic concentrator
cgt	cover glass tube
ct	concentric tube
e	outlet of collector
f	working fluid
gt	glass tube
in	inlet of collector
ict	inner copper tube
igt	inner glass tube
oct	outer copper tube
std	standard CPC
sim	simplified CPC

the conversion of low-grade heat sources including solar energy driven by steam less than 150 °C. Pei et al. [16] designed an innovative solar thermal electric generation system combined regenerative Organic Rankine Cycle (ORC) and CPC. Medium temperature solar steam can even sever as auxiliary heat for combined cycles [17]. All the above mentioned systems can serve as distributed power supplies in remote areas and small communities due to its inherent advantages.

Solar refrigeration technologies could be used for air-conditioning, ice making and refrigeration [18]. In general, solar thermally driven refrigeration technologies can mainly be divided into two categories: sorption technology and solar-driven ejector refrigeration. Sorption refrigeration usually requires a lower temperature heat source than ejector systems and requires steam pressure ranging from 0.1 to 1.0 MPa and temperature being in the range of 120–180 °C [19]. Pollerberg et al. [20] proposed a solar driven steam jet ejector chiller worked with medium temperature steam generated by PTC, which can generate cold water for air-conditioning. Cabrera et al. [21] studied an absorption chiller using double-effect cycles which can use medium temperature sources (140–180 °C). Berger et al. [22] also proposed a two cascading ammonia water absorption chiller driven by pressurized steam in 160–200 °C that can produce cold temperatures down to −12 °C. Their results suggested that solar steam in medium temperature and relatively high pressure can be used for refrigeration through either absorption or ejection efficiently.

Apart from the traditional utilizations, solar steam can also be applied in more areas. In hospital, surgical instrumentation needs to be processed properly to prevent infection, in which the commonly used method is called immediate use steam sterilization (IUSS). IUSS requires superheated steam at 132 °C [23,24], which can be provided by solar steam generator. Superheated steam (SS) between 110 °C and 185 °C can also be used to decontaminate food products without significantly destroying the major nutrient levels [25,26].

The steam mentioned above can be generated by various solar collectors. Nixon et al. [27] and Kalogirou et al. [28] compared the commercially available solar collectors including PTC, CPC, linear Fresnel reflectors etc. The advantages and applied range of each system has been depicted. Zhang et al. [29–31] had studied steam in medium temperature (120–200 °C) and relative high pressure (0.10–0.75 MPa) generated by PTC with *U*-type solar receiver. However, considering costs, modularity and fabrication, CPC is chosen as solar collector in our configurations. CPC is a non-imaging, non-tracking and low-concentration ratio (less than 10) collector, which can accept both direct and diffuse radiation over a wide range for a given concentration ratio [32].

In the present paper, a novel solar steam generator has been proposed with simplified CPC characterized by low-cost, easy fabrication, simple operation and modularity. The generator can produce steam in a temperature range from 100 to 200 °C and pressure between 0.1 and 0.55 MPa, which has great potential in numerous applications not only including Industrial Process Heat, power generation, refrigeration, but even involving food processing and sterilization in hospitals. The solar steam generator primarily consists of 60 collecting units with a total aperture area of 32 m^2 and each unit comprises an all-glass evacuated tube, a simplified non-tracking compound parabolic concentrator (CPC) and a metal concentric annular tube. Outdoor experimental studies have been performed to investigate the actual performance of the designed solar steam generator in summer time under different operating conditions.

2. Experimental apparatus and procedure

2.1. Experimental apparatus

Figs. 1 and 2 show the schematic of the solar steam generator system and its photograph respectively. The entire experimental configuration consists of four main parts as illustrated in Fig. 1,

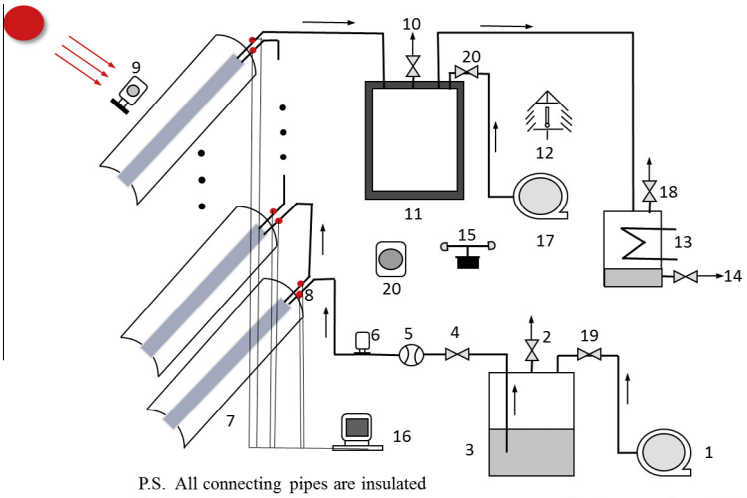

P.S. All connecting pipes are insulated

1. Air pump
2. Safety valve
3. Water supply tank
4. Flow control valve
5. Flow meter
6. Pressure transmitter
7. CPC solar collector
8. Thermocouples(ϑ_{in}, ϑ_e)
9. Radiometer
10. Safety valve
11. Steam outlet stabilizing tank (insulated)
12. Ambient temperature sensor
13. Cooler
14. Condensed water discharging valve
15. Anemometer
16. Data acquisition system
17. Air pump
18. Relief valve
19,20. Control valve
21. Barometer

Fig. 1. Schematic of the integral experimental set up.

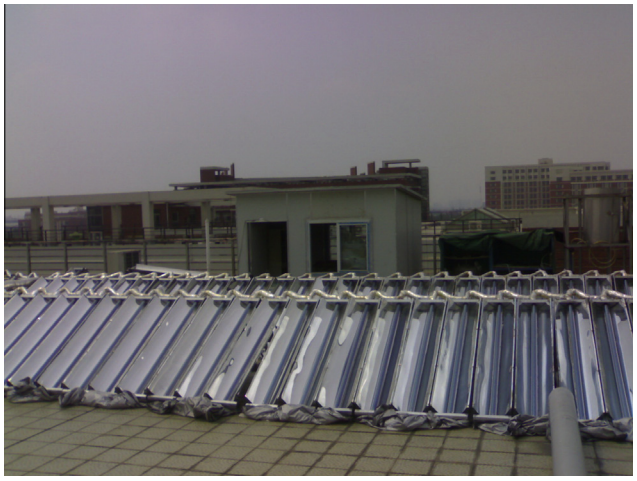

Fig. 2. A photograph of the experimental configuration.

including a high pressure water supply tank, solar collectors, a pressure stabilizing tank, and measuring system. The high pressure water supply tank is mounted at the inlet of collectors while the pressure stabilizing tank is at the outlet of the collectors. All connecting pipes in the apparatus are insulated and protected by a reflective weather proof coating to reduce thermal loss of the working fluid to ambient.

The high-pressure water supply tank with capacity of 500 L is mounted at the inlet of the collectors via a rubber tube. Initially, 240 L water is filled in the tank; then air is compressed into the tank by air pump until the pressure in the tank approaches required value. Afterwards, water can be compressed into the collector system and gradually heated after switching on the valve at the inlet. Flow rate of working fluid can be controlled by the flow control valve at the inlet of collectors. Meanwhile, inlet pressure can be measured by the pressure transmitter.

The solar collector for generating steam is composed of 60 sub collecting units in series. Each unit mainly consists of three components, including a simplified non-tracking compound parabolic concentrator (simplified CPC for short), an all-glass evacuated concentrator (glass evacuated tube) which is usually used in domestic solar water heater and a concentric metal annular tube inserted in the glass evacuated tube.

A decompression adjusting valve is mounted on the pressure stabilizing tank to regulate the back pressure inside the tank to a setting value. The pressure in pressure stabilizing tank is lower than that of the water supply tank in order to sustain consistent flow. In this study, different back pressures ranging from 0.10 to 0.55 MPa are tested, in order to generate saturated and superheated steam respectively. This tank can work in either barometric back pressure or high back pressure via controlling the decompression adjusting valve mounted on it. During the experiments, high back pressure is required and can be achieved using air pump, while the pressure inside the tank is stabilized by a safety valve.

The measuring system consists of thermocouples, air thermometers, pressure transmitters, flow meters, an anemometer (Testo 405), a radiometer (TES-1333R, TES electrical electronic corp.) and a barometer. All the measurement devices are mounted and conform to the ISO-9806 standard [33]. In the configuration, thermocouples are installed at the inlet and outlet of specified collector units, all the thermocouples shall be mounted at no more than 200 mm from the collector inlet and outlet; and insulation shall be placed around the pipe work both upstream and downstream of the sensor. Ambient air temperature is measured by an air thermometer which is shaded from direct and reflected solar radiation by means of a white-painted, well-ventilated shelter, preferably with forced ventilation and positioned aside the collectors with a distance less than 10 m. The mass flow rate is directly gauged by a flow meter mounted at the inlet of collectors. As is known, heat losses from collectors increase with increasing air speed over the collectors. In our tests, air speed is measured by an anemometer which is located beside the collector array; Due to constantly

changing air speed, a mean air speed is therefore adopted. As to the radiometer, it is mounted in a way that its sensor is coplanar with the collector plane within a tolerance of 1° and can receive the same levels of direct, diffuse and reflected solar radiation as received by the collector. Ambient pressure is measured by the barometer.

In addition, before the outdoor experiments, some pre-tests of the collecting system need to be done to evaluate if it conforms the ISO-9806 standard. According to the standard, the following tests are deployed: 1. Leakage test: the test is deployed to ensure no leakage along the flow path during the outdoor experiments. In the test, pressurized air is used as the working fluid through the collectors and two flow meters are mounted at the inlet and outlet of the collector respectively. The result shows that no appreciable difference of flow rates gauged by the two flow meters is detected, which can manifest good sealing of the apparatus. 2. Internal pressure tests for fluid channels: This test examines if the apparatus can withstand the pressures which it might meet in service. 3. External and internal thermal shocks: collectors may from time to time be exposed to sudden rainstorms on a hot sunny days or a sudden intake of cold heat transfer fluid on a hot sunny day, both of which will cause severe thermal shocks. The tests are intended to assess the capability of a collector to withstand such thermal shocks without a failure. 4. Rain penetration test is conducted for checking the thermal insulation layer.

2.2. The simplified CPC structure

CPC is characterized of larger acceptance angle, which can obviate the need for tracking the sun. This advantage makes CPC a desirable choice for collecting solar radiation. For the convenience of fabrication and assembly, a simplified stationary CPC is designed and fabricated based on the standard CPC structure shown in Fig. 3(a).

As illustrated in Fig. 3(b), the profile of simplified CPC at the bottom is a flat curve rather than an involute curve in a standard CPC. Furthermore, the designed CPC is truncated in order to obtain a larger acceptance angle and to reduce cost. According to the theoretical calculation and practical test, concentrating efficiency of the simplified CPC decreases by approximately 10–15% than a standard CPC. The simplified CPC reflector is made through bending a stainless steel mirror (2 mm thick) into the designed profile. The reflector is 330 mm in width and 146 mm in height, which is fixed explicitly to a sustaining shelf via two 60 mm-in-diameter holes in both the top and bottom ends of the shelf. Detailed characteristics of the designed CPC system are listed in Table 1.

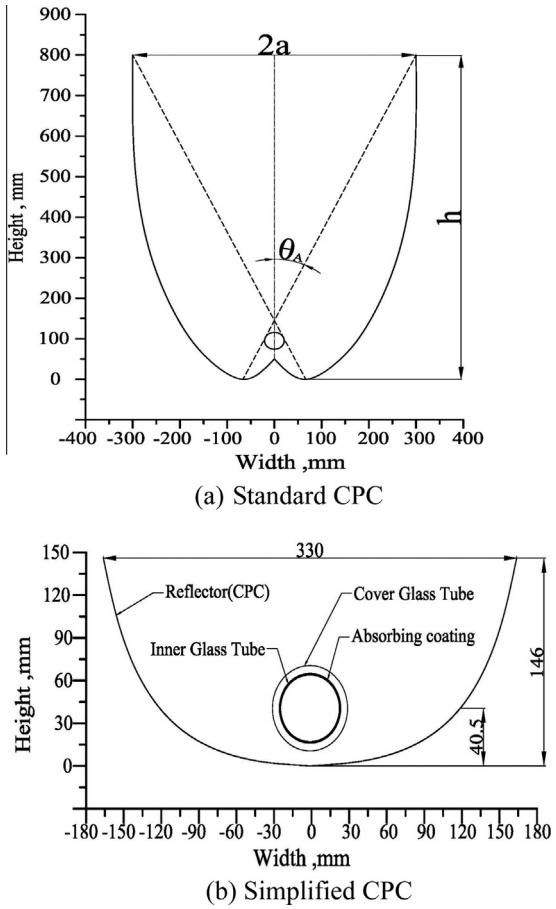

Fig. 3. Structure of standard CPC and simplified CPC.

2.3. All-glass evacuated tube

The all-glass evacuated tube is widely used as solar water heater concentrator for domestic hot water applications in China due to its low cost and exceedingly good collecting performance which can dramatically reduce thermal losses related to conduction, convection and radiation. The all-glass evacuated tube used in this study is provided by Sunshore Solar Energy Co., Ltd., which primarily consists of inner and outer tubes made of borosilicate glass, selective absorption layer, spring clip and getter as illustrated in Fig. 4 in detail. As is shown, the inner tube has an open end and is sealed with the outer tube in the evacuated annular region while enclosed at the other end in semispherical shape. A spring clip in the annular region at the other end sustains the inner tube and alleviates thermal stress caused by temperature variations. In addition, selective absorbing material is coated on the outer surface of the inner tube aiming to significantly reduce thermal radiation loss due to high temperature.

2.4. Copper concentric tube and heat transfer medium

A copper concentric tube inserted in the glass tube is used to heat water/steam flowing through the metal tube. The structure of concentric tube and fluid flow path are shown in Fig. 5. The concentric tube consists of two copper tubes which are welded together in the inner diameters of 20 mm and 32 mm respectively. The high conductivity of the copper tube can result in excellent circumferential temperature distribution and no appreciable bending

Table 1
Characteristics of the simplified CPC collector system.

Parameter	Value
Simplified CPC	
Width (w)	330 mm
Effective length (l_{CPC})	1600 mm
Height (h)	146 mm
Diameter of absorber (d)	48 mm
Acceptance half angle of standard CPC (θ_A, std)	8°
Acceptance half angle of simplified CPC (θ_A, sim)	65°
Reflectivity of CPC (ρ)	0.85
Concentration ratio (C_R)	2.16
Collector slope angle (φ)	30°(local latitude)
All-glass evacuated tube	
Diameter of Cover glass tube (d_{cgt})	58 mm
Diameter of Inner glass tube (d_{igt})	47 mm
Effect length of glass tube (l_{gt})	1600 mm
Concentric tube	
Diameter of outer copper tube (d_{oct})	20 mm
Diameter of inner copper tube (d_{ict})	32 mm
Effective length (l_{ct})	1500 mm
Thickness of copper tube (δ)	1 mm

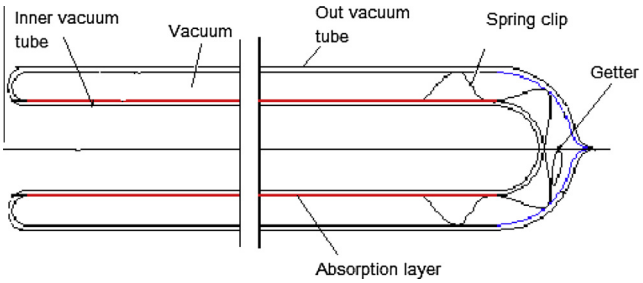

Fig. 4. Structure of glass vacuum tube.

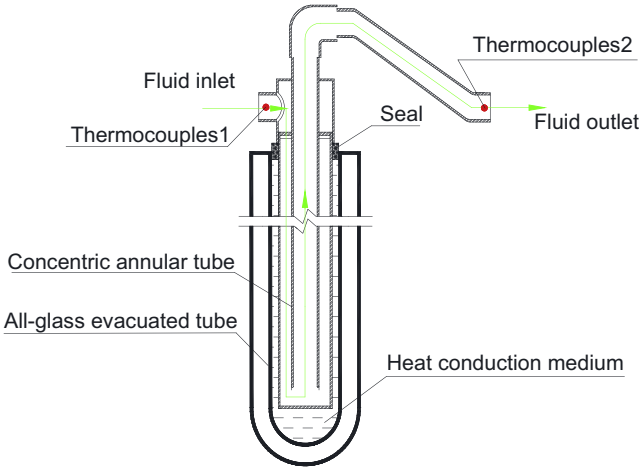

Fig. 5. Fluid flow path in concentric annular metal tube.

of the receiver [34,35]. Two annular tubes are connected by a thread cutting ferrule with polyethylene sealing adhesive tape. The working fluid, i.e., the mixture of water and steam enters the inlet then flows down to the bottom through the annular area of the annular tube. Meanwhile, the working fluid is continuously heated by heat medium surrounded outside the annular tube during the flow process. After that, the working fluid flows up through the core area of the annular tube at the bottom and exit from the outlet. During the flow process, the heated working fluid in the core area will release heat to the outer working fluid in the annular area. The geometric parameters of the concentric annular tube are listed in Table 1 in detail.

Heat transfer medium filled in the annular section formed by concentric annular tube and glass evacuated tube transfers heat absorbed by the selective layer to the working fluid; so its thermal properties greatly affect the collecting efficiency of the collector system. In addition, heat medium also acts as cushioning to protect fragile glass tubes from damage caused by thermal stresses. In the present paper, a paste-like oil–powder mixture (mixture of graphite powder and high temperature heat transfer oil) combining the advantages of oil and powder is developed. Different ratios of oil and powder are tested in an attempt to find the optimal ratio that has higher thermal conductivity, considerable low thermal expansion coefficient and long term thermal stability. Result shows that the optimal combination has a much higher heat conductivity of 0.629 W/m K than heat transfer oil (0.2 W/m K) and excellent thermal endurance.

3. Experimental methodology and error analysis

In order to acquire the all-day performance of the collectors, outdoor exposure experiments are conducted. The measurement methods and errors of measuring devices are all in accord with the ISO-9806 standard except the simulated steady solar radiation intensity. The experiments are conducted both in barometric and high back pressures.

Before every run, pure water of about 200 kg is charged into the water tank, after which air is compressed into the tank in advance until the inside pressure approaching 1.20 MPa. During the experiments, the volumetric flow rate of water is controlled by an adjusting valve and measured by a flow meter. Since the volume of the water tank is large enough and the mass decrease of water in the tank is small during the run, the volumetric flow rate of water almost keep constant. For the runs with high back pressures, the back pressure in stabilizing tank located at the system outlet is set by a decompression adjusting valve. The pressure transmitter used in the experiments has a standard uncertainty less than 0.5%.

Mass flow rate, $\dot{m}$, is determined through the measurement of volumetric flow rate, $\dot{V}$, with. $\dot{m} = \rho_f \cdot \dot{V}$, where ρ_f denotes density of working fluid, kg/m^3, pressure and temperature is measured during tests. The volumetric flow meter is calibrated over the range of fluid flow rates and temperatures of collector testing. The standard uncertainty of the volumetric flow rate measurement is within ±1%. The uncertainties are ±0.1 K for temperature measurement and ±50 Pa for pressure measurement of water passing through the inlet of the system. The result uncertainty of mass flow rate is less than ±2.0%.

The 1 mm sheathed *K*-type thermocouples are used in the experiments to measure temperatures of the working fluid at the collector, the wall of inner glass tubes and outer wall of the annular metal tubes in the collecting units. The temperature data is collected every 10 s automatically by Agilent34970 data acquisition system and transferred to computer. Every thermocouple is calibrated by standard thermometer with measuring error of ±0.1 K. In consideration of sealing and thermal insulation, thermocouples are only deployed at the inlet of the 5th, 6th, 12th, 13th, 19th, 20th and 40th to 60th units. Radiometer with an accuracy of ±4% specified by the manufacturer is used to measure the direct solar irradiation incident normal to the collector plane. The ambient air temperature is measured with a standard uncertainty less than 0.5 K. The speed of the surrounding air over the front surface of the collector is measured with a standard uncertainty of 0.01 m/s for outdoor testing. In this paper, the data from six typical runs are analyzed and the detailed experimental conditions are shown in Table 2.

4. Performance parameters

4.1. Instantaneous system power output and thermal efficiency

In general, performance tests of solar energy products are conducted under steady-state solar radiation intensity. However, the performance study of present solar steam generator is a developing and research experiment rather than a product test. In the study, all-day performance study has been evaluated outdoors under different weather conditions, flow rates and solar radiation intensities. It should be noted that all the data in the experiment has been collected instantaneously with a certain stable water/steam mass flow rate but transient solar radiation intensities.

Because the solar radiation changes with the time during day time, the performance of the system varies continuously. Instantaneous power output and the thermal efficiency are two very important and widely used parameters to evaluate the performance of the system.

The instantaneous system power output $\dot{Q}$ is calculated from:

$$\dot{Q} = \dot{m}(h_{f,e} - h_{f,in}) = \dot{m}\Delta h_f \quad (1)$$

where $\dot{m}$ is mass flow rate of working fluid, kg/s; $h_{f,in}$ is enthalpy of working fluid at the inlet of collector, J/kg; $h_{f,e}$ is enthalpy of

Table 2
Detailed experimental conditions of six typical runs.

Run date/time interval	Weather/ambient temperature (°C)	Inlet temperature(°C)/mass flow rate (kg/s)	Inlet/back pressure (MPa)	Saturation temperature (°C)	Average air speed (m/s)
2010-08-13/09:00–16:11	Sunny/39	26/3.33 × 10^{-3}	0.12/0.10	100	0.50
2010-08-02/08:34–15:16	Cloudy/39	26/3.33 × 10^{-3}	0.12/0.10	100	0.10
2010-08-19/09:40–15:57	Sunny/39	27/3.89 × 10^{-3}	0.12/0.10	100	0.25
2010-09-08/08:42–15:33	Sunny/36	25/3.33 × 10^{-3}	0.52/0.40	143	0.45
2010-09-09/08:50–15:41	Cloudy/36	25/3.33 × 10^{-3}	0.52/0.40	143	0.30
2010-09-16/08:56–15:08	Cloudy/34	25/3.33 × 10^{-3}	0.70/0.55	156	0.40

working fluid at the outlet of collector, J/kg, Δh_f is enthalpy difference of the collector inlet and outlet $\Delta h_f = h_{f,e} - h_{f,in}$.

The instantaneous system thermal efficiency η_{hem} [33] is defined as:

$$\eta_{hem} = \frac{\dot{Q}}{A_G \cdot G \cdot n} = \frac{\dot{m}\Delta h_f}{A_G \cdot G \cdot n} \tag{2}$$

where A_G represents the gross area of a single sub collector unit, m^2; G denotes the solar radiation intensity, W/m^2; n is the number of collector units.

For a specified system with a known optical efficiency of collector, the system thermal efficiency [36] may be rewritten as;

$$\eta_{hem} = \eta_{op} - \eta_{loss} = \eta_{op} - c \cdot (\Delta h_f / G) \tag{3}$$

where η_{loss} denotes the heat loss ratio; G is solar irradiance, W/m^2; c is a correlation factor which represents a relationship between the thermal loss and the enthalpy difference in the collector. For common solar air and water heaters, c can be reckoned as a proportionality constant of the enthalpy difference of working fluid.

The thermal efficiency intercept is the optical efficiency of the collector, when collecting temperature or enthalpy difference between the collector inlet and outlet is not obvious; for instance, for the first several collecting units, the unit efficiency is quite approximate to the optical efficiency.

4.2. Optical efficiency of the CPC collector

The optical efficiency of collector [37] is calculated by:

$$\eta_{op} = \rho \cdot \tau_e \cdot \tau_d \cdot \alpha_i \cdot p \cdot f_{ref} \tag{4}$$

According to the measured results, for the present experimental system, the reflectivity of CPC plate, ρ, is 0.8. The transmissivity of the evacuated tube, τ_e, is 0.9. The absorptivity of selective coating, α_i, is 0.92 and the dust stratification factor of evacuated tube, τ_d, is 0.9. The gap loss coefficient of simplified CPC type concentrator plate is given by the follows engineering calculation formula: $p = 1 - g/(\pi d)$ [38]. f_{ref}, here represents multiple reflection coefficients between cover glass tube and inner glass tube.

The absorptivity of the coating is measured in a room test and may be regarded as a constant of 0.92, while the emissivity of the coating ε_i changes along with the coating temperature. The relationship of emissivity and the temperature may be written as a correlation:

$$\varepsilon_i = 0.058 + 0.00041 \cdot T_i \tag{5}$$

According to the above-mentioned constants, the optical efficiency may be estimated as

$$\eta_{op} \approx 0.51 \tag{6}$$

5. Results and discussion

5.1. Effect of the number of collecting units on steam outlet temperature

As water flows past the heat-collecting system, it is heated unit by unit and its temperature rises gradually. There is a maximum temperature when the heat loss of the collector is equivalent to the solar radiation absorption. The outlet temperature of the working fluid is a complicated function of the solar radiation intensity and the construction of collector.

Fig. 6 shows the outlet temperatures of selected units, which is selected from the six typical runs and quite representative. The test is conducted on a sunny day with a maximum ambient temperature of 39 °C, and is operated with barometric back pressure. The mass flow rate of the working fluid is 3.33 × 10^{-3} kg/s.

As can be seen from the figure, the outlet temperatures of the working fluid at the 6th, 12th, 20th, 40th, 50th and 60th units are not monotonous with time; but depend on solar radiation intensity and the state of working fluid inside. With the increasing number of collecting units, the outlet temperature of each unit is continuously increasing. When the number of units is less than 20, the outlet temperature of the last unit can only stay a little higher than the saturated steam line corresponding to the back pressure (100 °C) in a short time; and there is no steam generated in the last unit. When the number of the units reaches 40, the superheated steam will be generated at the outlet of the last unit in a short time at noon. For the whole system consisted of 60 units, the superheated steam will be generated at the outlet of the last unit in about 3 h at noon. Considering the state of the working fluid inside the whole system, it can be divided into three periods which

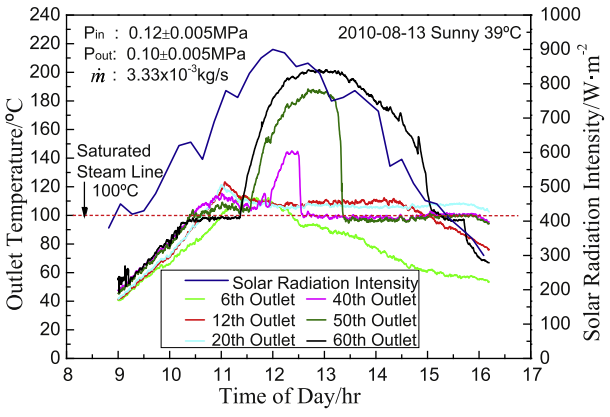

Fig. 6. Outlet temperatures of specified collecting units (2010-08-13).

are water, saturated steam and superheated steam. The working fluid may be heated to saturate state at about 11:00 am in most of the collector units. In other words, the collecting system now is mostly filled with moist steam. At about 11:20 am, the outlet temperature of the 60th unit begins to increase and the system starts to generate superheated steam. From then on, the last 20 heat collecting units are all full of superheated steam. It also can be seen from the figure that the maximum steam outlet temperature of the 60th, 50th and 40th units can be up to 202, 186 and 144 °C, respectively. However, in the afternoon the temperature of steam generated by the system declines rapidly and the system outlet temperature drops to saturation temperature at 15:00 pm because of decreased solar radiation intensity. According to experimental results, the steam outlet temperature is able to keep steady above 150 °C within 3 h at noon and the whole system could produce saturated steam in nearly 6 h consistently for the present system with 60 sub collector units.

Fig. 7 shows the outlet temperatures of every measured unit at 12:10 pm when the solar radiation intensity is highest on that day. The outlet temperature increases very slowly with the increasing number of units for the former 40 units and then rises sharply for the latter 20 units. It should be noted that since there exists a pressure difference along the flow path and hence the saturated temperatures of working fluid inside the former units are higher by about 10 K than those corresponding to the back pressure. It is seen that the outlet temperature of the working fluid begins to reach the corresponding saturation temperature after the 12th units. Afterwards, working fluid begins to transform into wet steam or superheated steam.

As we all know, the heat absorbed in a fixed temperature increase by the working fluid is proportional to its mass rate and the whole collecting area. For the mass flow rate of 3.33×10^{-3} kg/s, the number of the units taken as 60 is reasonable for summer season. If continuatively increasing the number of collector units, the outlet temperature of the working fluid will hardly increase and reach a limited value. For any other mass flow rate, it just needs to add or release collecting units proportionally to achieve the same performance, regardless of that whether it is in series or in parallel. It can be concluded that adding collecting units for the whole system will not enlarge the outlet temperature, because the outlet temperature for the last few units stays stable after the working fluid reaches 200 °C. When the working fluid achieves such a temperature, heat loss radiated by the sub collector will be equal to heat gained by the sub collector, resulting in such an equilibrium temperature.

According to the performance of the above mentioned collecting components, relationships among the collecting efficiency of each unit, temperature of the selective coating and solar radiation intensity is calculated and shown in Fig. 8. Given the limited space, the calculation details would not be shown here [37]. Since the coating temperatures in different units are different, resulting in different collecting efficiencies in different units. It can be concluded from the figure that under a fixed radiation intensity, the higher the coating temperature is, the lower the efficiency of the collecting unit is. As to the last few units, the coating temperature approaches 200 °C. When solar radiation intensity is 800 W/m^2, the efficiency of the collecting unit is only 0.22 in theory. According to the measured results, the outlet temperature of the working fluid is 10 °C lower than the coating temperature in the same unit. So, this quite cost-effective system can provide about 200 °C steam with an acceptable efficiency in summer. If the system is operated at a higher temperature, the efficiency would drop drastically due to the inherent disadvantages of non-tracking CPC.

5.2. Effect of back pressure on the performance of system

Fig. 9 shows the outlet temperatures of the working fluid in specified measuring units at a high back pressure run on a sunny day in summer. The experimental data can be compared with those at barometric back pressure shown in Fig. 6 in order to investigate the effect of back pressure on the outlet temperatures of the working fluid at different units under the same mass flow rate and the same basic solar radiation intensity.

In the figure, at about 11:00 am, water is only heated to its saturation temperature; working fluid in the latter 20 units still stays in wet steam state. At 11:50 am, the outlet temperature arises and the system starts to generate superheated steam; meanwhile temperatures in the 40th and 50th units commence to go up leading working fluid in the last 20 units to superheated state. When solar radiation reaches its maximal at 12:40 pm, the system would approach its highest outlet temperature in 190 °C, while the maximum outlet temperatures at the 40th and 50th are 164°Cand 179 °C respectively. However, in the afternoon the steam outlet temperature declines rapidly and drops to saturation temperature at 14:30 owing to decreased solar radiation intensity. According to experimental results, the steam outlet temperature is able to keep above 150 °C for 2.5 h at noon consistently. Compared with Fig. 6, it can be found when the system is operated in high back pressure, the system still can acquire superheated steam near 200 °C with acceptable efficiency. However, both the maximum outlet

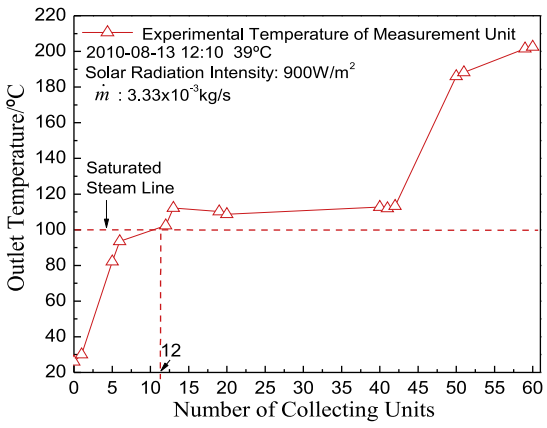

Fig. 7. Outlet temperatures of each unit under maximum solar radiation intensity.

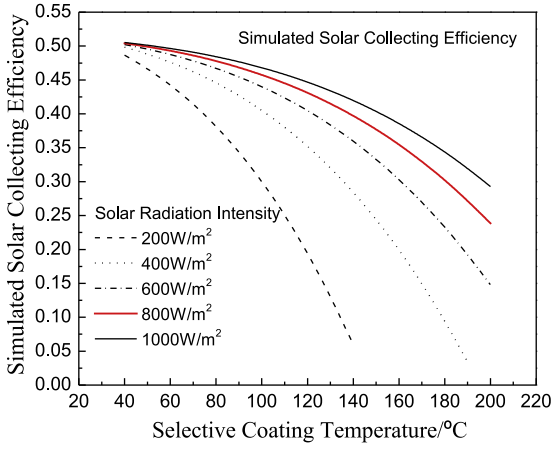

Fig. 8. Relationship between the collecting efficiency of each unit and coating temperature at different solar radiation intensities.

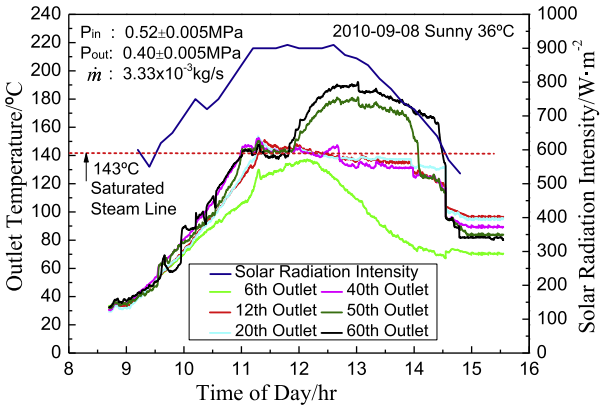

Fig. 9. Outlet temperatures of specified collecting units at a high back pressure run.

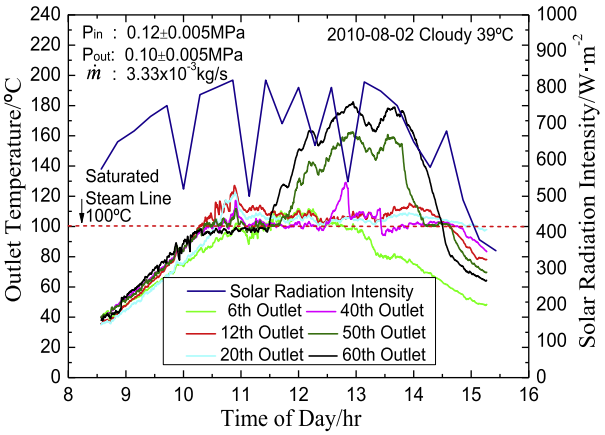

Fig. 10. Outlet temperatures at measuring units in a cloudy day at the atmospheric back.

temperature and time-lasting of steady steam are reduced due to the decreasing collecting efficiency in every unit.

5.3. Effect of weather conditions on system performance

Fig. 10 shows the outlet temperatures of the working fluid in specified measuring units in barometric back pressure run in a cloudy day in summer. The experimental data can be compared with those on a sunny day and a barometric back pressure shown in Fig. 6 to investigate the effect of weather on the outlet temperatures of the working fluid at different units under the same mass flow rate and back pressure.

Solar radiation will be blocked out in cloudy weather, resulting in a significant fluctuation in solar radiation intensity. It is obvious that the outlet temperature trend of working fluid is different from that of sunny days. Under this circumstance, the steam outlet temperature of the 60th, 50th and 40th units can only be up to 182,162 and 128 °C, respectively. Compared to Figs. 6 and 9, they are lower than that of sunny days due to the decrease of solar intensity.

In Fig. 10 at about 11:20 am, water is heated to its saturation temperature from the 12th unit. Working fluid thereafter is in wet steam state until 12:30 am, the outlet temperature arises and superheated steam is generated. Due to relatively lower solar radiation intensity, temperatures in the 40th units keep around the corresponding saturation temperature. The steam can attain a maximum outlet temperature of 162 °C owing to the relatively lower solar radiation intensity. On a cloudy day, solar radiation intensity is in waves and the mean solar radiation intensity is lower than that of a sunny day, resulting in lower collector efficiency refers to Fig. 6. Besides, the proportion of diffuse radiation which is hard to concentrate increases on a cloudy day. According to experimental results, the steam outlet temperature is able to keep steady above 100 °C within 3 h at noon and could produce saturated steam in nearly 4 h consistently for the present system with 60 sub collector units.

Fig. 11 shows the outlet temperatures of measuring units at 12:30 pm when the average solar radiation intensity approaches its maximal on that day. The outlet temperature is not increasing for the former 40 units and then rises sharply for the latter 20 units. The temperature of working fluid inside the system starts to reach the corresponding saturation temperature after the 12th units, which shows hysteresis compared to Fig. 6. The tendency of steam outlet temperature is very close to that of a sunny day as shown in Fig. 6.

5.4. Effect of wave of mass flow rate on outlet temperatures of units

Fig. 12 shows the experimental data of the water mass flow rate of 3.89×10^{-3} kg/s whose mass flow rate is 20% higher than the run shown in Fig. 6 under other same basic experimental conditions. By comparing the data shown Figs. 12 and 6, the effect of the mass flow rate on the outlet temperature in measuring units can be evaluated. As shown in Figs. 12 and 6, the two experiments have similar steam outlet temperature distribution and tendency. The maximum outlet temperature is nearly the same though the mass flow rate increases in 20%. However, the supply time of steady superheated steam is decreased from nearly 3 h to about 2.5 h. It may be reasonably speculated that the supply time of steady superheated steam can be increased if decreasing the mass flow rate of the working fluid. So the results confirm that increasing the mass flow rate by 20% has very limited influence on the maximum outlet temperature; but has significant influence on the supply time of steady superheated steam.

5.5. Power output of the system

In order to evaluate the whole day performance of the system, the instantaneous power output of the system is calculated and discussed. As shown in Eq. (1), instantaneous power output is the difference of total enthalpies of working fluid between inlet and outlet of the collector in a unit time. The power output of the system under two typical weather conditions is shown in Fig. 13. It can be seen that the tendency of power output is practically in accordance with that of solar radiation intensity. For barometric back pressure condition shown in Fig. 13(a), the power output of the system can exceed 9 kW on a cloudy day, and reach 11.12 kW at noon on a sunny day. Though the outlet temperature of the working fluid has a violent change with time, the change of

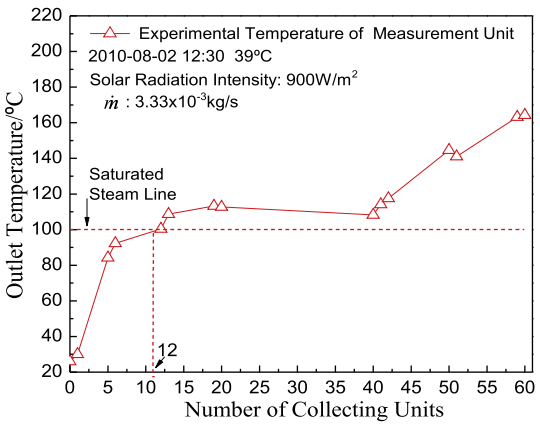

Fig. 11. Outlet temperatures of each unit under maximum solar radiation intensity.

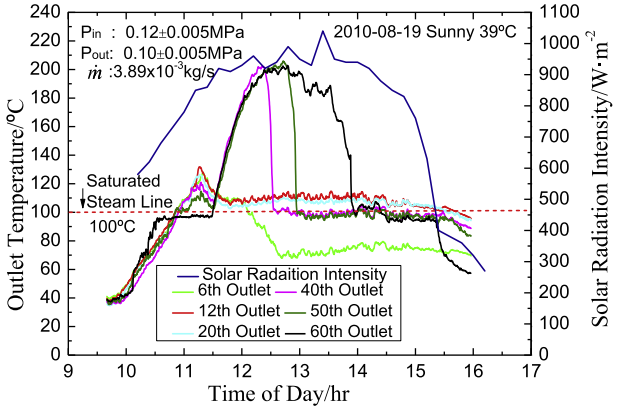

Fig. 12. Effect of wave of mass flow rate on outlet temperatures in measuring units.

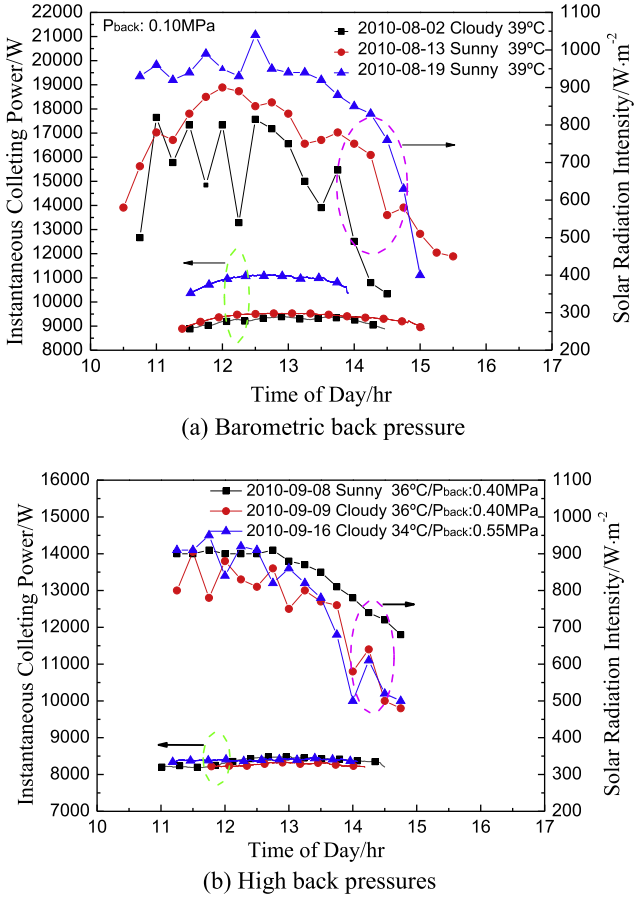

Fig. 13. Instantaneous collecting power distribution of collector during high temperature period.

the power output is flat for all day. The reason is that the sensible heat from the superheated steam is much less than the evaporating latent heat of the saturated steam and occupies only a small portion of the steam total enthalpy.

On other hand, for the high back pressure conditions as shown in Fig. 13(b), the power outputs of the system have slight decreased by 6% than that of barometric back pressure due to the increase of the coating temperature in the former units which leads to the decrease of the total thermal efficiency.

Moreover, though the average steam outlet temperature and solar radiation intensity on a cloudy day are less than those on a sunny day, the discrepancy of the power output between them is not evident due to lower operating temperature and higher thermal efficiency.

It also can be found that the solar radiation intensity changes dramatically from time to time, while the system power output merely fluctuates in a small range, said 0.5 kW. This phenomenon manifests that the system performance is not acutely fluctuated with solar radiation intensity and has a good damping characteristic due to using a special heat transfer medium filled in the annular section formed by concentric annular tube and glass evacuated tube which can act like a heat storage material. From the discussion above, it can be found that the performance of the solar collector has an intricate relationship with the working fluid temperature at the outlet and solar radiation intensity.

5.6. Mean system thermal efficiency

The system thermal efficiency is another important parameter to estimate the whole day performance of the system and is usually defined as the ratio of energy collected and solar radiation intensity incident to the CPC collector as shown in Eq. (2). The relationship of sub collector efficiency and the coating temperature under different solar radiation intensity for every unit has been presented in Fig. 8 and it has a strong and complicated coupling relationship with the coating temperature in every unit. In general, for common solar air and water heaters, the system thermal efficiency may be represented as an empirical correlation of the enthalpy difference of the working fluid between the inlet and the outlet, the radiation intensity and the optical efficiency of collector as shown in Eq. (3) since the radiation heat loss has a similar proportional relationship with the enthalpy difference of the working fluid between the inlet and outlet. In the present work, the mean system thermal efficiency corresponding to the mean solar radiation intensity during 45 min is plotted in the form of Eq. (3) based on the experimental data obtained in the three typical sunny runs with different mass flow rates and back pressures. These data are obtained according to the ISO-9806 standards.

Fig. 14 gives out the relationship between the mean system thermal efficiency and the ratio of the enthalpy difference to the mean solar radiation intensity around noon in sunny days. It is clearly demonstrated that the system thermal efficiency decreases with increasing enthalpy difference between the inlet and the outlet, while it increases with increasing solar radiation intensity. The thermal efficiency intercept is the optical efficiency of collector whose estimated value is equal to about 0.51 for the present system. Since the maximum outlet enthalpy or outlet temperature of steam always corresponds to the maximum solar radiation intensity at noon, the sole effects of the both outlet enthalpy and solar radiation intensity cannot be shown in this fitting method.

The experimental data may be fitted as a linear relationship,

$$\overline{\eta_{hem}} = 0.51 - 4.50 \times 10^{-5}(\Delta h_f / G) \tag{7}$$

where G is mean solar radiation intensity, W/m^2 and Δh_f is enthalpy difference of the collector inlet and outlet, J/kg.

In the present experiments, the minimum value of the mean system thermal efficiency is about 0.32 with corresponding steam outlet temperature of about 200 °C, which is quite close to the maximum temperature of steam for the present system. All system thermal efficiencies around noon in the experiments are greater than 30% for all sunny days with solar radiation intensity larger than 650 W/m^2. These thermal efficiencies for such a low-cost steam generator system are quite high compared to the results in other studies.

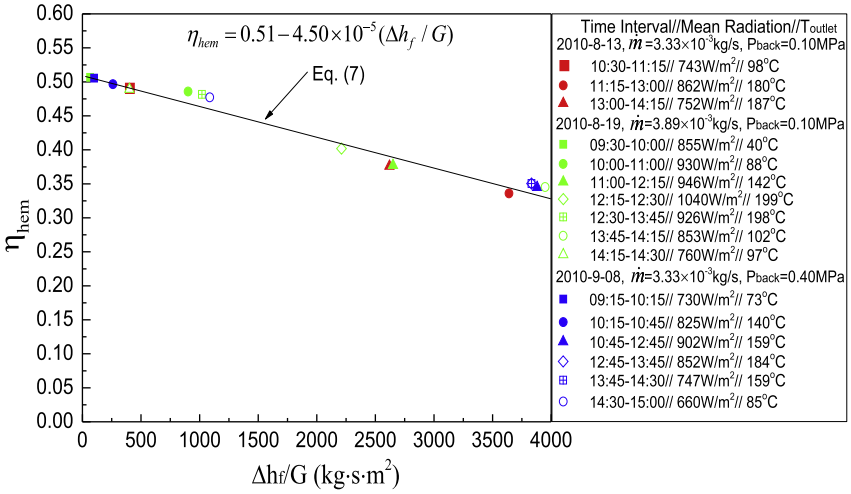

Fig. 14. Relationship between mean system efficiency and ratio of enthalpy difference to solar radiation intensity around noon.

6. Conclusions

A novel evacuated tubular solar steam generator with simplified CPC (Compound Parabolic Concentrator) and concentric annular tube heat exchanger is designed and tested to provide steam with moderate temperature in the back pressure range of 0.10–0.55 MPa. Experimental results show that high pressure and barometric pressure steam over 200 °C can be acquired during the experiments with an average efficiency above 0.30 on sunny and cloudy days in summer. Over 150 °C superheated steam can be effectively generated continuously for 3 h at noon and nearly 6 h for saturated steam. The present solar steam generator is consisted of 60 collecting units with a total aperture area of 32 m^2 and can output power of 8–11 kW for 3 h at noon. These results manifest that the present experimental system is of good collecting performance and would be a promising solar steam generator used in various solar thermal applications.

Acknowledgements

Financial supports from the National Basic Research Program of China (973 Program) through Project No. 2013CB228303 and National Natural Science Foundation of China through Grant No. 51276113 are gratefully acknowledged.

References

[1] IEA. Key World Energy Statistics. International Energy Agency, 2013.
[2] Mekhilef S, Saidur R, Safari A. A review on solar energy use in industries. Renew Sustain Energy Rev 2011;15(4):1777–90.
[3] Kalogirou S. The potential of solar industrial process heat applications. Appl Energy 2003;76(4):337–61.
[4] Thomas A. Solar steam generating systems using parabolic trough concentrators. Energy Convers Manage 1996;37(2):215–45.
[5] Zahler C, Iglauer O. Solar process heat for sustainable automobile manufacturing. Energy Proc 2012;30:775–82.
[6] Calderoni M, Aprile M, Moretta S, Aidonis A, Motta M. Solar thermal plants for industrial process heat in Tunisia: economic feasibility analysis and ideas for a new policy. Energy Proc 2012;30:1390–400.
[7] Beath AC. Industrial energy usage in Australia and the potential for implementation of solar thermal heat and power. Energy 2012;43(1):261–72.
[8] García-Rodríguez L, Palmero-Marrero AI, Gómez-Camacho C. Application of direct steam generation into a solar parabolic trough collector to multieffect distillation. Desalination 1999;125(1–3):139–45.
[9] Gudekar AS, Jadhav AS, Panse SV, Joshi JB, Pandit AB. Cost effective design of compound parabolic collector for steam generation. Sol Energy 2013;90:43–50.
[10] Fernández-García A, Zarza E, Valenzuela L, Pérez M. Parabolic-trough solar collectors and their applications. Renew Sustain Energy Rev 2010;14(7):1695–721.
[11] Mittelman G, Epstein M. A novel power block for CSP systems. Sol Energy 2010;84(10):1761–71.
[12] García-Rodríguez L, Blanco-Gálvez J. Solar-heated Rankine cycles for water and electricity production: POWERSOL project. Desalination 2007;212(1–3):311–8.
[13] Ho T, Mao SS, Greif R. Comparison of the organic flash cycle (OFC) to other advanced vapor cycles for intermediate and high temperature waste heat reclamation and solar thermal energy. Energy 2012;42(1):213–23.
[14] Almanza R, Lentz A. Electricity production at low powers by direct steam generation with parabolic troughs. Sol Energy 1998;64(1–3):115–20.
[15] Ferrara G, Manfrida G, Pescioni A. Model of a small steam engine for renewable domestic CHP (combined heat and power) system. Energy 2013;58:78–85.
[16] Pei G, Li J, Ji J. Analysis of low temperature solar thermal electric generation using regenerative Organic Rankine Cycle. Appl Therm Eng 2010;30(8–9):998–1004.
[17] Luo C, Zhang N. Zero CO_2 emission SOLRGT power system. Energy 2012;45(1):312–23.
[18] Abdulateef JM, Sopian K, Alghoul MA, Sulaiman MY. Review on solar-driven ejector refrigeration technologies. Renew Sustain Energy Rev 2009;13(6–7):1338–49.
[19] Sarbu I, Sebarchievici C. Review of solar refrigeration and cooling systems. Energy Build 2013;67:286–97.
[20] Pollerberg C, Ali AHH, Dötsch C. Solar driven steam jet ejector chiller. Appl Therm Eng 2009;29(5–6):1245–52.
[21] Cabrera FJ, Fernández-García A, Silva RMP, Pérez-García M. Use of parabolic trough solar collectors for solar refrigeration and air-conditioning applications. Renew Sustain Energy Rev 2013;20:103–18.
[22] Berger M, Weckesser M, Weber C, Döll J, Morgenstern A, Häberle A. Solar driven cold rooms for industrial cooling applications. Energy Proc 2012;30:904–11.
[23] Nania P. Immediate use steam sterilization: it's all about the process. AORN J 2013;98(1):32–8.
[24] Hutzler L, Kraemer K, Iaboni L, Berger N, Bosco 3rd JA. A hospital-wide initiative to eliminate preventable causes of immediate use steam sterilization. AORN J 2013;98(6):597–607.
[25] Cenkowski S, Pronyk C, Zmidzinska D, Muir WE. Decontamination of food products with superheated steam. J Food Eng 2007;83(1):68–75.
[26] Head DS, Cenkowski S, Arntfield S, Henderson K. Superheated steam processing of oat groats. LWT – Food Sci Technol 2010;43(4):690–4.
[27] Nixon JD, Dey PK, Davies PA. Which is the best solar thermal collection technology for electricity generation in north-west India? Evaluation of options using the analytical hierarchy process. Energy 2010;35(12):5230–40.
[28] Kalogirou SA. Solar thermal collectors and applications. Prog Energy Combust Sci 2004;30(3):231–95.
[29] Zhang L, Yu Z, Fan L, Wang W, Chen H, Hu Y, et al. An experimental investigation of the heat losses of a *U*-type solar heat pipe receiver of a parabolic trough collector-based natural circulation steam generation system. Renew Energy 2013;57:262–8.
[30] Zhang L, Wang W, Yu Z, Fan L, Hu Y, Ni Y, et al. An experimental investigation of a natural circulation heat pipe system applied to a parabolic trough solar collector steam generation system. Sol Energy 2012;86(3):911–9.
[31] Zhang L, Fan L, Hua M, Zhu Z, Wu Y, Yu Z, et al. An indoor experimental investigation of the thermal performance of a TPLT-based natural circulation steam generator as applied to PTC systems. Appl Therm Eng 2014;62(2):330–40.
[32] Winston R. Principles of solar concentrators of a novel design. Sol Energy 1974;16(2):89–95.
[33] International Standard ISO-9806. Solar energy–solar thermal collectors-test methods first edition. 2013.

[34] Almanza R, Lentz A, Jiménez G. Receiver behavior in direct steam generation with parabolic troughs. Sol Energy 1998;61(4):275–8.
[35] Roldán MI, Valenzuela L, Zarza E. Thermal analysis of solar receiver pipes with superheated steam. Appl Energy 2013;103:73–84.
[36] Gang P, Guiqiang L, Xi Z, Jie J, Yuehong S. Experimental study and exergetic analysis of a CPC-type solar water heater system using higher-temperature circulation in winter. Sol Energy 2012;86(5):1280–6.
[37] Wang P-Y, Guan H-Y, Liu Z-H, Wang G-S, Zhao F, Xiao H-S. High temperature collecting performance of a new all-glass evacuated tubular solar air heater with U-shaped tube heat exchanger. Energy Convers Manage 2014;77:315–23.
[38] Rabl A. Optical and thermal properties of compound parabolic concentrators. Sol Energy 1976;18(6):497–511.